Electrochemical and Electrostatic Cleavage of Alkoxyamines

Long Zhang,[a,b] Eduardo Laborda,[c] Nadim Darwish,*[,a] Benjamin B. Noble,[d] Jason H. Tyrell,[d] Sandra Pluczyk,[e] Anton P. Le Brun,[f] Gordon G. Wallace,[b] Joaquin Gonzalez,*[,c] Michelle L. Coote,*[,d] and Simone Ciampi*[,a]

[a] Department of Chemistry, Curtin University, Bentley, Western Australia 6102, Australia
[b] ARC Centre of Excellence for Electromaterials Science, Intelligent Polymer Research Institute, University of Wollongong, Wollongong, New South Wales 2500, Australia
[c] Department de Quimica Fisica, Universidad De Murcia, Murcia 30003, Spain
[d] ARC Centre of Excellence for Electromaterials Science, Research School of Chemistry, Australian National University, Canberra, Australian Capital Territory 2601, Australia
[e] Department of Physical Chemistry and Technology of Polymers, Silesian University of Technology, Gliwice 44-120, Poland
[f] Australian Centre for Neutron Scattering, Australian Nuclear Science and Technology Organization (ANSTO), Lucas Heights, NSW 2234, Australia

ABSTRACT: Alkoxyamines are heat-labile molecules, widely used as *in-situ* source of nitroxides in polymer and materials sciences. Here we show that the one-electron oxidation of an alkoxyamine leads to a cation radical intermediate that even at room temperature rapidly fragments releasing a nitroxide and carbocation. Digital simulations of experimental voltammetry and current-time transients suggest the unimolecular decomposition which yields the "unmasked" nitroxide (TEMPO) is exceedingly rapid and irreversible. High-level quantum computations indicate the collapse of the alkoxyamine cation radical is likely to yield a neutral nitroxide radical and a secondary phenylethyl cation. However, this fragmentation is predicted to be slow and energetically very unfavorable. To attain qualitative agreement between the experimental kinetics and computational modelling for this fragmentation step the explicit electrostatic environment within the double layer must be accounted for. Single-molecule break-junction experiments in a scanning tunneling microscope using solvent of low dielectric (STM-BJ technique) corroborate the role played by electrostatics forces on the lysis of the alkoxyamine C–ON bond. This work highlights the electrostatic aspects played by charged species in a chemical step that follows an electrochemical reaction, defines the magnitude of this catalytic effect by looking at an independent electrical technique in non-electrolyte systems (STM-BJ), and suggests a redox on/off switch to guide the cleavage of alkoxyamines at an electrified interface.

INTRODUCTION

Electrostatic catalysis refers to the use of static electric fields to catalyse ordinary chemical reactions.[1] Conversion of reactants into products is synonymous of electronic reorganization, yet little is known on the effect of static charges on chemical catalysis. Chemists appreciate that redox currents at electrodes respond predictably to changes in voltage – for instance a bias of about one Volt pointing in the right direction can lead to changes in redox currents by a factor of up to 10^8. These currents are the manifestation of the rate at which electrons are either lost or gained; hence the field-effect is easily explained and accounted for. On the other hand, the effect of static electricity on non-redox reactivity, long suggested by theoretical chemists,[2] is not intuitive and it is just starting now to emerge as an important branch of chemical catalysis.[1, 3] The chemical implications are expected to be broad since electrolytes and electrostatic interactions are ubiquitous in chemical, material and biological sciences,[2c, 4] to the point of dominating the entire reaction space in natural or technological environments, such as cell membranes,[5] fluidic channels[6] or the confined electrolyte space of a porous electrode.[7]

The theories and models describing the role of electrostatic forces on the formation or rupture of chemical bonds were pioneered by Pocker,[8] Bertrán,[2c] Warshel[9] and Shaik[10] starting from the 1970s. This form of catalysis arises because formally covalent species can be stabilized via minor charge-separated resonance contributors. A non-polar covalent bond A–B might be written as [A–B $\leftrightarrow$ A^+–B^- $\leftrightarrow$ A^-–B^+], but in the absence of an electrostatic force A–B is dominant and the extent of resonance stabilization is small. Only in the presence of an appropriately-oriented electric field one of the charge-separated contributors can be stabilized. The electrostatic "awakening" of the ionic character of bonds, and the effect on reaction barriers that follows can be dramatic.[1, 3b, 11] The obvious and perceived challenge is how to align molecules and field so as to take advantage of these effects.[3b, 12]

The present experiments were initially designed as an attempt to harness electrostatic catalysis in nitroxide-mediated polymerization. Previously we had shown that the electric field from remote negatively charged functional groups could dramatically lower the bond dissociation energy of alkoxyamines and facilitate their homolysis at temperatures lower than otherwise possible.[12a, 13] The catalytic effect is delivered by the charges of ionized functional groups and can therefore be predictably

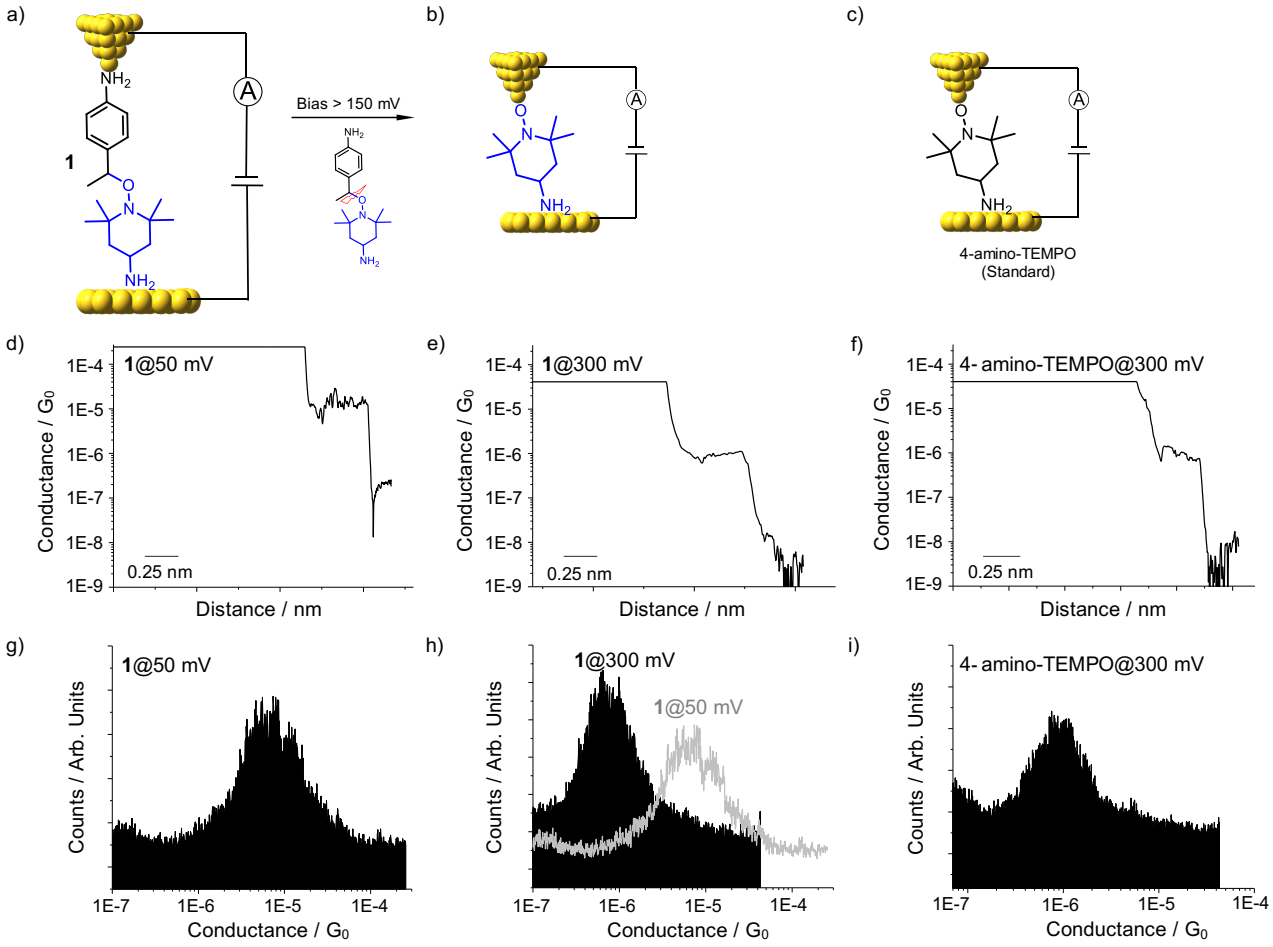

Figure 1. Electrostatic catalysis in the homolysis of alkoxyamines. (a-c) Schematic depiction of the STM-BJ setup for a single-molecule junction experiment used to investigate the effect of an external electrical field on the breaking of a C–ON bond. We used single-molecule STM-BJ conductance measurements to probe the fate of the alkoxyamine molecule **1** under a variable electric field stimulus in a low dielectric solvent. The experiments capture discrete electrical signals from either the intact parent molecule **1** or from the putative 4-amino-TEMPO fragment that is produced upon the homolysis of **1**. A STM tip is brought into and out of contact with an Au(111) surface while this is covered with a diluted solution of the molecule of interest (either **1** or a 4-amino-TEMPO standard in mesitylene/DCM, 10:1, v/v). The surface is biased against the tip and the current versus distance signal is collected as the tip is moved away from the surface. (d-f) Typical current versus distance traces with conductance plateaus indicative of a single-molecular junction. The current drops from the current-saturation value to the current-amplifier detection limit, passing through breakage steps, "plateaus", each of a specific conductance value. (g-i) Conductance histograms showing the electrical "fingerprints" of either the intact alkoxyamine **1** (i.e. before splitting, tip-surface bias < 150 mV) at 1E-5 G_0 ($G_0 = (2e^2/h$ = 77.5 µS, quantum of conductance) or the free nitroxide that is unmasked after splitting (bias > 150 mV) at 1E-6 G_0. The molecular conductance obtained upon homolysis of **1**, as shown in (h, **1**@300 mV), is a perfect match of the results from control experiments where the two electrodes are forming junctions in a standard sample of commercial 4-amino-TEMPO (c,f,i).

adjusted according to pH.[13a] The electric field that is associated with these charges alters the stability of charge-separated resonance contributors (N–O$^{\bullet}$ ↔ N$^{+\bullet}$–O^{-}) and hence the extent of stabilization of the nitroxide. This ultimately leads to electrostatic catalysis of reactions involving such "switchable" nitroxides, including alkoxyamine dissociation and hydroxyl amine hydrogen transfer. However, whilst this electrostatic effect is large in the gas phase,[12a] in solution it progressively diminishes as the polarity of the solvent increases.[13b] Further, whilst this type of pH switch is possible in solvents of low polarity,[13a] its practical use here is hampered by the low solubility of charged species, leading to a trade-off between solubility

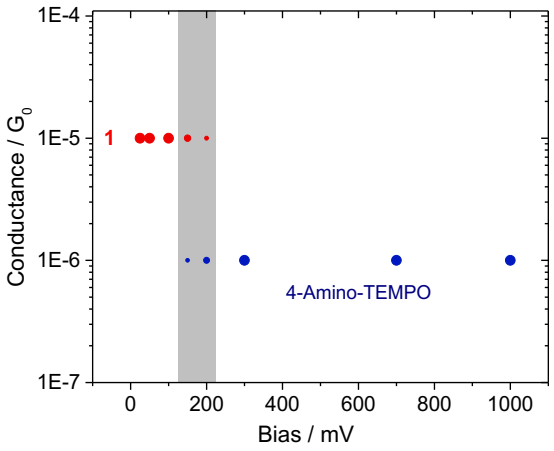

Figure 2. Electric fields and breaking probability of single-molecules. The plot shows the effect of the bias between the STM tip and the Au(111) surface over the fate of several thousand molecular junctions (*ca*. 4000 for each data point) each obtained by electrically "wiring" molecules of alkoxyamine **1** in a STM-BJ experiment. At biases in the range between 150 and 200 mV, discrete conductance plateaus at both 1E-5 G_0 and 1E-6 G_0 appear, reflecting the co-existence of both the parent molecule **1** and its homolysis product (4-amino-TEMPO). The area of each data point reflects the relative bias-dependent abundance of the species.

and magnitude of the electrostatic catalytic effect.

This raises the question as to whether there is a better and more general method of introducing charges and ensuring they align with reaction axes. One strategy that we have successfully used relies on electrification of molecules while these are held under bias in the nanoscale gap between metal electrodes of a scanning tunneling microscope-break junction (STM-BJ) set-up. STM-BJ is the only technique available to bring together single molecule reactants between nanoscale electrodes, it is unparalleled in its ability to deliver a large oriented electric field (V/nm) which is here tunable and can catalyze several thousands of chemical events over short periods of time. Using STM-BJ (in mesitylene as solvent) we have recently demonstrated a link between electrostatic forces and the rate of formation of a carbon–carbon covalent bond.[3b] However, it remains that while this technique can be key in an experimental scrutiny leading to proof-of-concept data, it is clearly not practical to process workable quantities of materials in STM-BJ.

A simpler approach, suitable for unimolecular reactions at least, is to attach a molecule to an electrode. Previously we have shown that nitroxides can be grafted onto highly-doped, i.e. metallic, Si(100) electrodes;[14] in the present work we use a similar monolayer-chemistry method to graft alkoxyamines. In this way reactants can be aligned the double layer of electrochemical cells. Moreover, by tethering an alkoxyamine to an electrode we hoped to use nitroxide mediated polymerization to grow surface-tethered polymer with narrow molecular weight distributions in a manner that was both spatially and temporally controlled.

In what follows we first use STM-BJ to demonstrate that an external electric field triggers homolysis of alkoxyamines at room temperature. We then show that in an electrochemical cell at an appropriate voltage, alkoxyamines also undergo room temperature cleavage, irrespective of whether they are tethered to an electrode or not. However, we show that the latter process is actually an ECE (electrochemical-chemical-electrochemical) process whereby the alkoxyamine is first oxidised prior to rapid cleavage into a nitroxide and carbocation, followed by oxidation of the nitroxide. Interestingly, the chemical step itself is nonetheless driven by electrostatic effects, even when the alkoxyamine is not tethered to a surface suggesting self-alignment in the double layer is possible and that directional electrostatic effects are possible in solution and may be an important and often overlooked contributing factor in organic electrochemistry.

RESULTS AND DISCUSSION

Electrostatic Cleavage of Alkoxyamines in a Single-Molecule Scanning Tunneling Microscope Break-Junction Experiment. To establish whether electrostatic effects can trigger alkoxyamine homolysis we conducted STM-BJ experiments. The repetitive formation of molecular junctions in the STM-BJ technique is an established method of accessing conductance measurements on single-molecules.[15] It also allows access to a statistically significant pool of data on bond breaking (and/or reformation[3b]) in response to changes in field magnitude. We have explored the role of electric fields on the lysis of alkoxyamines by bridging a molecule (alkoxyamine **1**, Figure 1a) between a gold STM tip and an Au(111) substrate under a bias stimuli of variable magnitude. Alkoxyamine **1** is symmetrically substituted with primary amino groups at opposite ends of the molecule (see Supporting Sections S1 and S2 for synthetic procedures). These two primary amine pendants have affinity toward gold, allowing electrical contacts to be made with the reactant, *i.e*. molecules of **1**, by both the STM Au tip and the Au(111) surface. The single molecule conductance is measured by repeatedly forming and breaking the molecular junction by "tapping" the STM tip in and out of contact with the Au(111) surface while this is covered by a diluted sample of **1** (in mesitylene/DCM, 10:1, v/v solvent). Current plateaus appear in the pulling curves reflecting the formation of a single-molecule junction. By means of accumulating thousands of individual current-distance traces, (Figure 1d-f), we built conductance histograms (Figure 1g-i) showing peak maxima that reflect the most probable conductance value of the molecule(s) in the junction at a given tip–surface bias.

Figure 2 summarizes visually the outcome of STM-BJ experiments on **1**. In brief, below a threshold bias of 150 mV the statistical analysis of individual plateaus in the current versus distance curves leads to a single prominent peak in the conductance histogram at *ca*. 1E-5 G_0 (where $G_0 = 77.5$ μS). This peak is unambiguously assigned to the parent alkoxyamine, indicating the presence exclusively of intact molecules of **1** in the electrified gap (left column in Figure 1). Between 100 mV and 200 mV, however, a second plateau appears at 1E-6 G_0. Finally, above 300 mV, the 1E-5 G_0 peak disappears completely to be replaced by a 1E-6 G_0 electrical signature (Figure 2 and panels e and h in Figure 1). This conductance signature at 1E-6 G_0 is assigned to nitroxide species that are generated from the electric

field-induced splitting of **1** by a bias > 150 mV. Nitroxides have a known affinity for gold surfaces,[16] and the same 1E-6 G_0 conductivity signature is observed in control STM-BJ experiments that are performed using a standard 4-amino-TEMPO solution (right column in Figure 1). Moreover, unlike for the alkoxyamine **1**, STM-BJ experiments performed only in the presence of 4-amino-TEMPO molecules do not show a dependency of molecular conductance on bias, and for instance the conductance/G_0 ratio of these controls is unchanged between 50 mV and 300 mV (see panels c-d in Supporting Figure S1). It appears therefore extremely unlikely that the 1E-6 G_0 signature in this field-assisted lysis of **1** is arising from chemical entities other than a free nitroxide fragment. For example, STM-BJ control experiments of 4-vinylaniline (*i.e.* a putative end product of the homolysis[17]) are shown in panels e-f of Supporting Figure S1 and carry no evidence of any sizable peak in conductance histogram. The STM tip-to-substrate bias appears therefore to guide the redistribution between an alkoxyamine-only population (up to ca 100 mV of dc bias between STM tip and substrate) to a mixed alkoxyamine/nitroxide population (between 150 and 200 mV) and ultimately to a nitroxide-only presence (bias over 300 mV).

The role of the electric field in promoting the homolysis of the alkoxyamine can be explained by a theoretical model of the system. Quantum-chemical calculations of the reaction profile in the presence of a field of varying strength that is aligned along the N–O bond axis suggest that the homolysis of **1** is possibly promoted by as much as 35 kJ mol^{-1}. This barrier-lowering effect is consistent with the expected stabilization of the charge-separated resonance contributor to the nitroxide radical (N–O$^{\bullet}$ ↔ $N^{+\bullet}$–O^{-}) and is enough to account for the radical formation. Electrostatic effects can thus promote homolysis of alkoxyamines and can explain the observed STM results. However, it is difficult to extract truly quantitative theoretical data on the field/barrier relationship. This is because, while we clearly can control in STM-BJ the alkoxyamine/nitroxide population, the upper limit of the experimental electric field (V/nm) in the STM experiment is nonetheless relatively difficult to quantify as the distance between the tip and the Au(111) plate varies during the tapping experiments. Therefore, as a conservative measure, the range of field strengths considered in the theoretical model are probably a lower estimate (Supporting Section S7).

Electrochemical Cleavage. While the STM experiments provide proof of concept that electric fields can trigger alkoxyamine homolysis, they do not offer a practical route to chemical synthesis. So, we next explored whether electrostatic effects could instead be harnessed in an electrochemical cell. Chemists appreciate that the condition of bulk electro-neutrality is not valid at interfaces, and strong field gradients are ubiquitous at electrode/electrolyte interfaces (Debye layers).[4a, 18] Anodization of a surface-tethered alkoxyamine **2** in a perchlorate-based electrolyte (**S-1** surface construct in Figure 3, surface modification and XPS/XRR characterizations in Supporting Scheme S2 and Supporting Figures S2 and S3, respectively) shows the gradual appearance of a TEMPO redox signature[14, 19] upon positive biases. A similar electrochemical pre-treatment with negative bias has only a minor effect on the cleavage. Under these conditions, the greater yield with positive bias was unexpected as the alkoxyamine (and product nitroxide radical) is tethered with the nitrogen-side of the polar $N^{\delta+}$–$O^{\bullet\delta-}$ bond closest to the electrode,

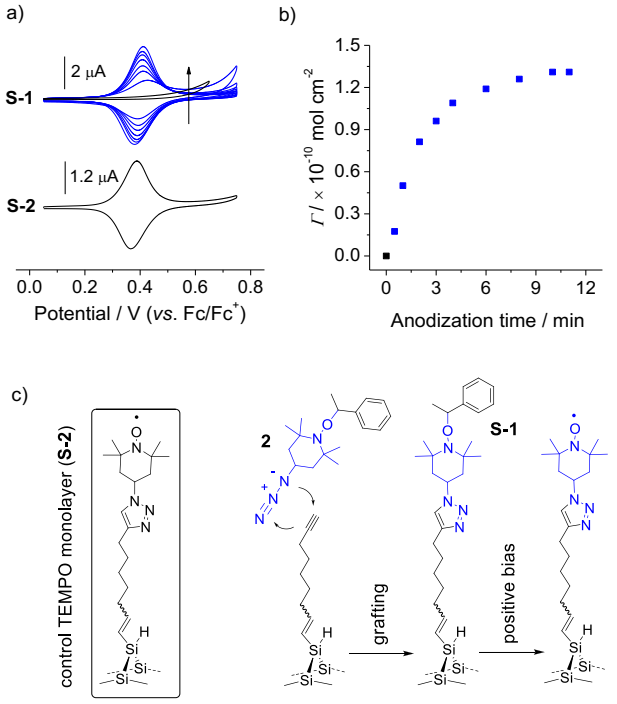

Figure 3. Anodic cleavage of a surface-tethered alkoxyamine (**S-1**) and its conversion into a Si(100) nitroxide-terminated monolayer (electrolyte is 1.0 × 10^{-1} M Bu_4NClO_4 in MeCN). The monolayer distal-end of **S-1** samples is the phenylethyl portion of an alkoxyamine molecule (**2**) and it is lost to the electrolyte upon electrolysis. (a) Cyclic voltammograms (100 mV s^{-1}) acquired before (black trace) and after (blue trace) applying a positive bias to **S-1** samples prepared on Si(100) electrodes. The potential is stepped from open circuit to 0.65 V (vs. Fc/Fc^+) for a 30 s period before recording a voltammogram and selected traces are presented in figure (blue traces). Anodization of **S-1** results in the progressive appearance of a redox signature that is in good agreement with that of a surface-tethered TEMPO control (**S-2**, black trace). The TEMPO coverage rises in increments of about 2.6 × 10^{-11} mol cm^{-2}, and reaches a maximum of ca. 1.31 × 10^{-10} mol cm^{-2}, equivalent to ca. 25% of a close-packed TEMPO monolayer assembled on a gold surface.[20] (b) Plot of the electrochemically-determined changes to the surface coverage of redox-active nitroxide radicals as a function of the anodization time of **S-1** samples. (c) Reaction schematics for the alkoxyamine surface model (**S-1**) and controls (**S-2**)

hence we had initially assumed that a negative electrode would better stabilize the nitroxide radical product. However, follow up diffusive experiments revealed that the situation is much more complicated than we first anticipated (*i.e.* simple stabilization of charge-separated contributors by distal negative

charges) and that in electrolytes the positive bias was actually leading to oxidation of the alkoxyamine. This in turn led to its

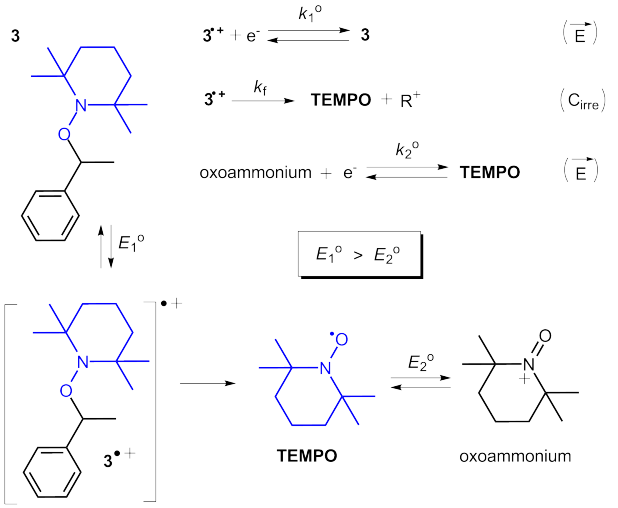

Scheme 1. Consecutive $EC_{irre}E$ mechanism accounting for the anodic fragmentation of alkoxyamines. The anodic intermediate (**3**$^{\bullet+}$) is an unstable transient species which is found to undergo rapid unimolecular decomposition (C_{irre}, k_f in the order 10^6 s^{-1}, details on individual electrolyte systems in the Supporting Information) releasing at room temperature the redox-active nitroxide fragment (TEMPO).

cleavage to a carbocation and nitroxide, followed by oxidation of the latter to oxoammonium (Scheme 1). We subsequently saw this same behavior in non-surface tethered nitroxide radicals, where digital simulations of voltammetry and *in-situ* electrochemical EPR experiments were able to help validate an $EC_{irr}E$ mechanism and measure the thermodynamic and kinetic parameters of the process. Figure 4a and Supporting Figures S4-S7 show representative experimental voltammograms, current-time transients (chronoamperometry) and digital simulations for the electrochemical oxidation of **3** at platinum electrodes in MeCN/Bu_4NClO_4 solutions. Extensive data sets where the voltage sweep rate and concentration of the alkoxyamine reagent were varied over two orders of magnitude range, respectively, are in Supporting Figures S5-S6.

The first anodic segment is featureless, *i.e.* it displays only a capacitive-like current until the potential is expanded to about 0.7 V, where the current raises rapidly to show a clear oxidative wave before the onset of background processes. This anodic process is irreversible over the time scale of the experiment. The lack of a back peak in cyclic voltammetry (Figure 4a), as well as the modelling of current-time transients (triple potential step chronoamperometry data in Figure S7), indicate the electron-transfer step is followed by a fast follow-up homogeneous chemical reaction. A satisfactory fit of both types of experiments does not require inclusion a second-order backward process in the chemical step, hence it is apparent that alkoxyamine **3** undergoes fragmentation after its initial electrochemical oxidation with a rather large chemical rate (k_f = 5.0 × 10^6 s^{-1}). The current magnitude of the most anodic wave as well as the appearance of a redox signature upon scan reversal both indicate that one of the two fragments is electrochemically-active. The electrode kinetics and thermodynamics for this fragment are a

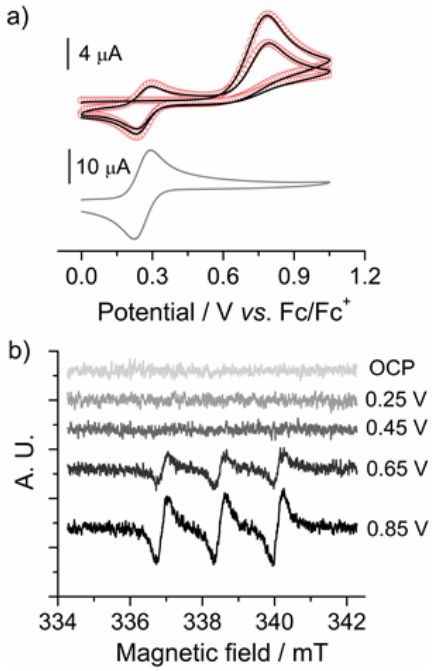

Figure 4. Anodic electrochemistry of alkoxyamines **3** at platinum electrodes. (a) Experimental (solid lines) and simulated (empty symbols) cyclic voltammograms of 0.5 × 10^{-3} M **3**, and experimental data (offset grey trace) of 0.5 × 10^{-3} M TEMPO controls. The best-fit parameters are *D* (**3**/**3**$^{\bullet+}$) = 7.8 × 10^{-6} cm^2 s^{-1}, *D* (TEMPO/oxoammonium) = 2.2 × 10^{-5} cm^2 s^{-1}, E_1^0 = 0.78 V, k_1^0 = 0.05 cm s^{-1}, E_2^0 = 0.195 V, k_2^0 = 0.08 cm s^{-1}, k_f = 5.0 × 10^6 s^{-1}. (Electrolyte is 1.0 × 10^{-1} M MeCN/Bu_4NClO_4, and scan rate is 100 mV s^{-1}, 0.7 cm^2 platinum macrodisk electrode). (b) In-situ electrochemical EPR measurements conducted in 1.0 × 10^{-1} M DCM/Bu_4NPF_6 in the presence of 0.5 × 10^{-3} M of **3**. The specified electrolysis bias (labels to curves vs. Fc/Fc$^+$) was imposed to a platinum wire electrode for 360 s with the EPR data being accumulated over the last 60 s of the potential step.

perfect match of those obtained for control experiments using TEMPO solutions (E^0_{TEMPO}= 0.21 V *vs.* Fc/Fc$^+$, k^0_{TEMPO} = 0.08 cm s^{-1}, lower grey trace in Figure 4a and extensive data sets in Supporting Figures S4 and S8). These controls, in conjunction with *in-situ* electrochemical EPR data (Figure 4b and Supporting Figure S9[21]) indicate that lysis of the oxidized alkoxyamine (**3**$^{\bullet+}$) is most likely occurring on its C–ON bond with release of the parent nitroxide (*i.e.* TEMPO, *vide infra* for the discussion on a quantum model of the system). In brief, digital simulations of the electrochemical data lead to the following main conclusions: i) the overall mechanism needs to be analyzed as an $EC_{irre}E$ process (*i.e.* sequential electrochemical-chemical-electrochemical steps, Scheme 1); ii) a large cation radical decay reaction rate constant (k_f) is needed to reproduce the shapes of all

the experimental curves; iii) the anodic wave at ca. 0.7 V includes two one-electron processes, the oxidation of **3** (refined E_1^0 = 0.78 V) and the oxidation of a portion of the newly-formed TEMPO units (refined E_2^0 = 0.195 V). In brief, after the oxidation of the parent alkoxyamine, $\mathbf{3}^{\bullet+}$ participates in a fast homogeneous chemical reaction explaining the mechanistic framework that leads to a free nitroxide and a carbocation at the electrified interface ($\mathbf{3}^{\bullet+} \rightleftarrows$ TEMPO + R^+, $k_b \rightarrow 0$).

Electrostatic Catalysis? The experimental finding that alkoxyamines, normally stable at room temperature, undergo rapid and irreversible room temperature homolysis upon oxidation is remarkable when analyzed in terms of the expected energetics of the process. High-level *ab initio* calculations were conducted at a level of theory previously demonstrated to reproduce experimental redox potentials of nitroxides[22] and homolysis equilibrium constants of neutral alkoxyamines[23]. The computed oxidation potentials versus Fc/Fc^+ of **3** (0.83 V) and TEMPO (0.20 V) in this work are also in excellent agreement with the corresponding best-fit experimental values (E_1^0= 0.78 V and E_2^0 = 0.195 V). Moreover, the calculations predict the correct preferred fragmentation pattern (*i.e.* to a nitroxide and carbocation rather than an oxoammonium cation and a carbon centered radical) further validating their accuracy. However, when the energetics of the homolysis of the oxidized alkoxyamine is calculated in MeCN it is unfavorable by 35 kJ mol^{-1}, a finding that is inconsistent with the rapid decomposition observed experimentally.

Importantly, the calculations only take account of the solvent and fail to consider the electric fields experienced in the near-surface double-layer. When these were taken into account, it is then clear that the homolysis is promoted (Figure 5). For instance, by using only a simple background electric field of 0.5 V nm^{-1}, a value which reflects the potential gradient that is most likely experienced by species reaching the electrified interface,[24] the homolysis energies were lowered but not by enough to explain the experimentally observed reaction rates. However, combination of a static electric field and a continuum solvent model (in which the solvent is itself modelled as an electric field) is likely to provide a rather crude approximation of the true environment. Unfortunately modelling a full ensemble of explicit ions and solvent molecules while maintaining a suitably high level of theory is impractical. However, we can show that when either an explicit ion or an explicit solvent molecule is included in the calculations, further lowering is observed (Figure 5). Hence it is most likely that the electrostatic environment within the double-layer is helping to promote homolysis of a compound that would otherwise be stable.

While the calculations suggest that the environment in the double layer is promoting homolysis, it is difficult to establish whether this is due to explicit bonding interactions or electrostatics as full ensemble of species cannot be modelled accurately (*vide supra*). To examine whether the effects were primarily electrostatic, experiments were thus conducted with anions that are significantly less coordinating than perchlorate, such as hexafluorophosphate and tetrakis[3,5-bis(trifluoromethyl)phenyl]borate (BARF hereafter) (see Supporting Figures S10-S14). The results are in line with the observations in the perchlorate system, pointing to an $EC_{irr}E$ mechanism with the backward chemical reaction not being operative in the time scale of the experiments. For example, with scan rates that varied over three orders of magnitude (from 75 mV s^{-1} to 8 V s^{-1}, Supporting Figure S13) the refinement of the voltammograms of alkoxyamine **3** in BARF electrolytes (k_f = 5.2 × 10^6 s^{-1})

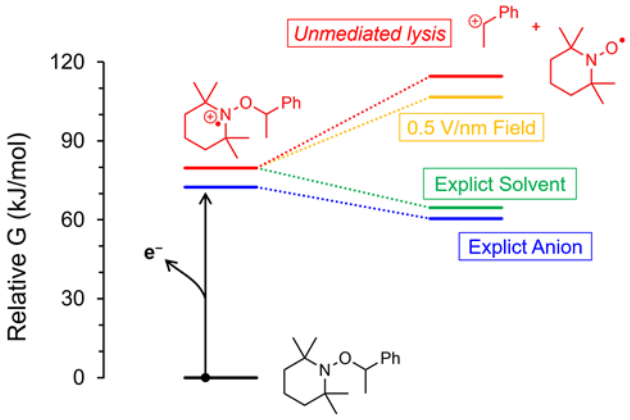

Figure 5. Theoretical potential energy surface for the oxidative cleavage of alkoxyamine **3** in MeCN. The homolysis of the unperturbed ('free') radical-cation (red pathway) is strongly thermodynamically disfavoured. However, homolysis can be made more favourable by a static electric field, and by interactions with an explicit anion and/or with an explicit solvent molecule.

suggest kinetic, as well as mass transport, parameters that are a close match of those obtained in Bu_4NClO_4 electrolytes (k_f = 5.0 × 10^6 s^{-1}) (Figures S5). Within the same solvent, the results remained unchanged (see Supporting Figure S5, S10 and S13), however, there were small differences between solvents (MeCN versus DCM, see Supporting Figure S5 and Figure S15). Indeed, this was also backed by theoretical calculations (Supporting Figure S19). Collectively, the experiments suggest that it is primarily the electrostatic environment in the double layer driving cleavage rather than explicit covalent interactions with the electrolyte ions.

CONCLUSION

Two areas of chemistry that are attracting increasing attention at present are the use of electrochemical reactions in organic synthesis, so-called synthetic organic electrochemistry,[25] and the use of static electric fields to catalyse non-electrochemical reactions, so-called electrostatic catalysis.[1-3, 12a, 13] The present work sits at the intersection of these fields. We have explored the prospect of using electricity and electrostatics as alternative triggers of alkoxyamine decomposition. In STM-BJ experiments we have shown that static electric fields can trigger alkoxyamine dissociation to nitroxides and carbon-centred radicals under conditions where they would otherwise be stable, while in the electrochemical experiments we have demonstrated an alternative means of homolysis, albeit to nitroxides and carbocations instead. We show that this latter reaction, an electrochemical $EC_{irr}E$ process, proceeds for free alkoxyamines in solution as well as for alkoxyamines tethered to a silicon elec-

trode, and can provide a convenient strategy for in situ generation of nitroxides and carbocations. Importantly, we show that even in the electrochemical process the C−ON cleavage step itself is only made possible by electrostatic effects, highlighting their previously overlooked role in organic electrochemistry.

EXPERIMENTAL SECTION

STM-BJ Measurement. Measurements of single-molecule conductivity using the STM-BJ technique were carried out using PicoSPM I microscope controlled by a Picoscan-2500 electronics (all from Agilent Technologies) and using a custom PTFE-STM cell for solid/liquid samples. The current versus distance curves (gold STM tip-to-Au(111) substrate distance) were captured using a NI-DAQmx/BNC-2110 National Instruments (LabVIEW) and analyzed with a LabVIEW code. The procedure of break-junction experiment is based on moving the STM tip to tunneling distance over an Au(111) surface that is covered with a dilute sample containing the molecules of interest (alkoxyamine **1**, 4-amino-TEMPO and 4-vinylaniline in mesitylene /DCM, 10:1, v/v). The STM current-feedback is then turned off and the tip is driven into and out of contact with the surface at a speed of ca. 50 nm/s. This 2-points cycle is repeated thousands of times enabling capturing of ca. 4000 distance versus current curves (current decays) for each set of data. Plateaus, indicative of the formation and subsequent rapture of single-molecule electrical junctions, appear during the pulling cycle of the externally driven 2 points loop. The current decays are then accumulated in conductance histograms. The peak maximum in the conductance histogram resemble the single-molecule conductivity of the sample (conductance (G) was calculated using the equation $G = I_{step}/V_{bias}$, where I_{step} is the plateau current and V_{bias} is the voltage difference between the tip and surface).

Electrochemical Methods and Digital Simulations. Electrochemical experiments were carried out using a CH 650D electrochemical analyzer (CH Instruments, Austin, TX) and a single compartment three-electrode PTFE cell. Platinum disks or chemically-modified Si(100) surfaces (**S-1** and **S-2** in Figure 3 and Supporting Scheme S2) served as the working electrode (analysis of diffusive systems of alkoxyamine **3** or surface-tethered models using alkoxyamine **2**, Scheme 1 and Figure 3, respectively), a platinum coil was used as counter electrode, and a plastic body silver/silver chloride "leakless" as the reference electrode (eDAQ, part ET072-1). The active area of the platinum disk was electrochemically-determined prior to each experiment from the refinement of a E model against experimental voltammogramms measured in 1.0×10^{-1} M $MeCN/Bu_4NClO_4$ in the presence of 0.5×10^{-3} M mM ferrocene (Fc in shorthand hereafter). The geometric area of the Si(100) working electrode was defined to 28 mm^2 by a Viton® gasket of rectilinear cross-section. The backside of the silicon sample was scratched with emery paper and rubbed with gallium-indium eutectic. A planar copper plate was pressed against the sample backside and served as ohmic contact. The reference electrode was calibrated before and after each experiment against the apparent formal potential of the ferricenium/ferrocene couple (Fc^+/Fc) at a platinum disk electrode in 0.5×10^{-3} M Fc. All potentials are reported against the Fc^+/Fc couple. Electrochemical experiments were performed at room temperature (23 ± 2 °C) in a grounded Faraday cage under argon. *In-situ* electrochemical EPR spectra were acquired in a cylindrical cell equipped with a platinum wire as a working electrode (2.5 cm length and 0.2 mm diameter), a platinum coil as an auxiliary electrode and a silver wire as a pseudo-reference electrode. The experiments were conducted using a JEOL JES-FA 200, X-band CW-EPR spectrometer operating at 100 kHz field modulation coupled with the Ecochemie AUTOLAB Autolab PGSTAT302N+BA potentiostat-galvanostat. During measurement the microwave power was equal to 0.995 mW and modulation width was equal to 0.1 mT and the influence of modulation width on registered spectra was also verified. Digital simulations of cyclic voltammetry and chronoamperometry experiments were performed in DigiElch-Professional v7 (ElchSoft). Simulated kinetic, thermodynamic and transport parameters for the electrode reaction were determined from fittings of experimental data sets that covered a range of concentrations assuming an $EC_{irre}E$ mechanism. Butler-Volmer kinetics was used to estimate charge transfer parameters. A semi-infinite 1D diffusion was assumed at both macrodisk planar and cylindrical electrodes (chronoamperometry in EPR experiments). For microdisks we considered semi-infinite 2D diffusion fronts with 27 (X) and 23 (Y) grid points. The cell iR drop was not compensated during measurement. Values of cell resistance were measured by electrochemical impedance spectroscopy and used in the simulations (data of resistance are: 140 Ω for $MeCN/Bu_4NPF_6$, 144 Ω for $MeCN/Bu_4NClO_4$, 1466 Ω for MeCN/NaBARF, 1220 Ω for DCM/Bu_4NPF_6, with the exception of the borate salt, which is present at 1.0×10^{-2} M, all supporting salts are at a concentration of 1.0×10^{-1} M). Adsorption steps were neglected in the simulations and the transfer coefficients for both electrons transfer reactions (TEMPO/oxoammonium and $\mathbf{3}/\mathbf{3}^{\bullet+}$) were assumed as constants (α, 0.5) for fitting purposes. Including a DISP-COMP pathway[26] does not improve the results. In the simulation the homogeneous chemical step for the fate of the putative benzylic cation fragment (R^+) was not considered as this has no effect on the quality of the fits. The diffusion coefficients of **3** and $\mathbf{3}^{\bullet+}$ were obtained from the best-fits of an $EC_{irre}E$ model of the linear sweep voltammogram at platinum microdisk electrodes and were assumed equal. For the chemical step, only the forward (k_f) constant is considered. The second-order backward (k_b) constant tends to zero (i.e. backward chemical reaction is not operative in the time scale of the experiments).

Computational Methods. Full details of all theoretical procedures use for simulating both the STM experiments and electrochemical experiments are provided in the Supporting Information, sections S7 and S8 respectively.

For the STM experiments, the principle aims were to study the effect of external electric field (EEF) on the reaction energies, rather than assess absolute reaction energies. For this purpose the M06-2X/6-31+G(d) as the level of theory, which has been benchmarked and used in previous studies of EEFs,[3b] was sufficient. Full conformer searching and geometry relaxation of each species was performed and the lowest energy conformer then used for subsequent calculations involving fields. Solvation energies in mesitylene solvent were calculated with the SMD solvent model, and all calculations were performed in Gaussian 09.[27]

For the electrochemical experiments, accurate absolute values of the oxidation potentials and homolysis energies were re-

quired and so higher levels of theory were used, based on extensive benchmarking studies, including for alkoxyamine homolysis energies,[23] and nitroxide oxidation potentials and ion-pairing energies.[14, 22] All geometry optimizations and frequency calculations were performed at the M06-2X/31+G(d,p) level of theory. Entropies, thermal corrections and zero-point vibrational energies were scaled by recommend scale factors.[28] Improved single-point energies were calculated using the high-level composite *ab initio* G3(MP2,CC)(+) method, a variation of standard G3(MP2,CC)[29] where calculations with the 6-31G(d) basis set are replaced with corresponding 6-31+G(d). These high-level calculations where utilized in conjunction with the ONIOM approximation[30] for larger systems, with either standard G3(MP2,CC) or UMP2 used to model remote substituents effects. The solvation model based on density (SMD)[31] was used to relax gas-phase structures to the solution-phase (at the UM06-2X/6-31+G(d,p) level of theory). Free energies of solvation were then calculated on solution-phase geometries using the COSMO-RS model,[32] using the ADF package,[33] at the BP/TZP level of theory (as it was parameterized for), and the remaining parameters were kept as default values[34]. All standard *ab initio* molecular orbital theory, density functional theory (DFT) calculations were carried out using Gaussian 09[27] and Molpro 2015[35] software packages.

ASSOCIATED CONTENT

Supporting Information

The Supporting Information is avaialble free of charge on the ACS Publications website at http://pub.acs.org.
Materials and methods, synthesis and characterization of molecules and chemically-modified S(100) surfaces, XPS and XRR spectra data, STM-BJ methods and additional data, extensive electrochemical data and simulations for diffusive systems, additional theoretical methods and results.

AUTHOR INFORMATION

Corresponding Authors

josquin@um.es
michelle.coote@anu.edu.au
nadim.darwish@curtin.edu.au
simone.ciampi@curtin.edu.au

ACKNOWLEDGMENTS

This work was supported by grants from the Australian Research Council (ARC, DE160100732 (S.C.), DE160101101 (N.D.), CE 140100012 (L.Z., B.B.N., M.L.C. and G.G.W), FL110100196 (G.G.W.)). J.G.S. and E.L. greatly appreciate the financial support provided by the Fundación Séneca de la Región de Murcia (Projects 19887/GERM/15 and 18968/JLI/13) and by the Ministerio de Economía y Competitividad (projects CTQ-2015-65243-P and CTQ-2015-71955-REDT). L.Z. would like to thank AINSE Ltd. for providing financial assistance. M.L.C. gratefully acknowledges allocations of supercomputing time on the National Facility of the Australian National Computational Infrastructure.

REFERENCES

(1) Shaik, S.; Mandal, D.; Ramanan, R. *Nat. Chem.* **2016,** *8*, 1091-1098.
(2) (a) Warshel, A. *J. Biol. Chem.* **1998,** *273*, 27035-27038; (b) Shaik, S.; Shurki, A. *Angew. Chem. Int. Ed.* **1999,** *38*, 586-625; (c) Sola, M.; Lledos, A.; Duran, M.; Bertran, J.; Abboud, J. L. M. *J. Am. Chem. Soc.* **1991,** *113*, 2873-2879.
(3) (a) Fried, S. D.; Bagchi, S.; Boxer, S. G. *Science* **2014,** *346*, 1510-1514; (b) Aragonès, A. C.; Haworth, N. L.; Darwish, N.; Ciampi, S.; Bloomfield, N. J.; Wallace, G. G.; Diez-Perez, I.; Coote, M. L. *Nature* **2016,** *531*, 88-91; (c) Geng, C.; Li, J.; Weiske, T.; Schlangen, M.; Shaik, S.; Schwarz, H. *J. Am. Chem. Soc.* **2017,** *139*, 1684-1689.
(4) (a) Parsegian, A. *Nature* **1969,** *221*, 844-846; (b) Warshel, A.; Levitt, M. *J. Mol. Biol.* **1976,** *103*, 227-249; (c) Novotny, J.; Sharp, K. *Prog. Biophys. Mol. Bio.* **1992,** *58*, 203-224; (d) Fried, S. D.; Bagchi, S.; Boxer, S. G. *J. Am. Chem. Soc.* **2013,** *135*, 11181-11192.
(5) Simon, M. L. A.; Platre, M. P.; Marquèsbueno, M. M.; Armengot, L.; Stanislas, T.; Bayle, V.; Caillaud, M.; Jaillais, Y. *Nat. Plants* **2016,** *2*, 16089-16123.
(6) Stein, D.; Kruithof, M.; Dekker, C. *Phys. Rev. Lett.* **2004,** *93*, 035901-035904.
(7) Feng, J.; Graf, M.; Liu, K.; Ovchinnikov, D.; Dumcenco, D.; Heiranian, M.; Nandigana, V.; Aluru, N. R.; Kis, A.; Radenovic, A. *Nature* **2016,** *536*, 197-200.
(8) Pocker, Y.; Buchholz, R. F. *J. Am. Chem. Soc.* **1970,** *92*, 2075-2084.
(9) Warshel, A. *Acc. Chem. Res.* **1981,** *14*, 284-290.
(10) Shaik, S. *J. Am. Chem. Soc.* **1981,** *103*, 3692-3701.
(11) Shaik, S.; Danovich, D.; Wu, W.; Hiberty, P. C. *Nat. Chem.* **2009,** *1*, 443-449.
(12) (a) Gryn'ova, G.; Marshall, D. L.; Blanksby, S. J.; Coote, M. L. *Nat. Chem.* **2013,** *5*, 474-481; (b) Gorin, C. F.; Beh, E. S.; Kanan, M. W. *J. Am. Chem. Soc.* **2011,** *134*, 186-189; (c) Akamatsu, M.; Sakai, N.; Matile, S. *J. Am. Chem. Soc.* **2017,** *139*, 6558-6561.
(13) (a) Klinska, M.; Smith, L. M.; Gryn'ova, G.; Banwell, M. G.; Coote, M. L. *Chem. Sci.* **2015,** *6*, 5623-5627; (b) Gryn'ova, G.; Coote, M. L. *J. Am. Chem. Soc.* **2013,** *135*, 15392-15403; (c) Gryn'Ova, G.; Smith, L. M.; Coote, M. L. *Phys. Chem. Chem. Phys.* **2017,** *19*, 22678-22683.
(14) Zhang, L.; Vogel, Y. B.; Noble, B. B.; Gonçales, V. R.; Darwish, N.; Brun, A. L.; Gooding, J. J.; Wallace, G. G.; Coote, M. L.; Ciampi, S. *J. Am. Chem. Soc.* **2016,** *138*, 9611-9619.
(15) (a) Xu, B.; Tao, N. J. *Science* **2003,** *301*, 1221-1223; (b) Chen, F.; Hihath, J.; Huang, Z.; Li, X.; Tao, N. *Annu. Rev. Phys. Chem.* **2007,** *58*, 535-564; (c) Tao, N. J. *Nat. Nanotechnol.* **2006,** *1*, 173-181.
(16) (a) Krukowski, P.; Kowalczyk, P. J.; Krzyczmonik, P.; Olejniczak, W.; Klusek, Z.; Puchalski, M.; Gwozdzinski, K. *Appl. Surf. Sci.* **2009,** *255*, 3946-3952; (b) Swiech, O.; Hrynkiewicz-Sudnik, N.; Palys, B.; Kaim, A.; Bilewicz, R. *J. Phys, Chem. C* **2011,** *115*, 7347-7354.
(17) (a) Tsuchimoto, T.; Tobita, K.; Hiyama, T.; Fukuzawa, S.-i. *J. Org. Chem.* **1997,** *62*, 6997-7005; (b) Noji, M.; Ohno, T.; Fuji, K.; Futaba, N.; Tajima, H.; Ishii, K. *J. Org. Chem.* **2003,** *68*, 9340-9347.
(18) Hurth, C.; Li, C.; Bard, A. J. *J. Phys. Chem. C* **2007,** *111*, 4620-4627.
(19) (a) Alévêque, O.; Seladji, F.; Gautier, C.; Dias, M.; Breton, T.; Levillain, E. *ChemPhysChem* **2009,** *10*, 2401-2404; (b) Alévêque, O.; Blanchard, P.-Y.; Breton, T.; Dias, M.; Gautier, C.; Levillain, E.; Seladji, F. *Electrochem. Commun.* **2009,** *11*, 1776-1780.
(20) Blanchard, P.-Y.; Alévêque, O.; Breton, T.; Levillain, E. *Langmuir* **2012,** *28*, 13741-13745.
(21) Supporting Figure 12 shows the simulated **TEMPO** concentration profiles and cumulative number of **TEMPO** molecules across the EPR cell obtained upon the anodization of **3**.
(22) Gryn'ova, G.; Barakat, J. M.; Blinco, J. P.; Bottle, S. E.; Coote, M. L. *Chem-Eur. J.* **2012,** *18*, 7582-7593.
(23) Hodgson, J. L.; Lin, C. Y.; Coote, M. L.; Marque, S. R. A.; Matyjaszewski, K. *Macromolecules* **2010,** *43*, 3728-3743.
(24) Yoon, Y. H.; Woo, D. H.; Shin, T.; Chung, T. D.; Kang, H. *J. Phys, Chem. C* **2011,** *115*, 17384-17391.
(25) (a) Yan, M.; Kawamata, Y.; Baran, P. S. *Angew. Chem. Int. Ed. Engl.* **2017**, DOI: 10.1002/anie.201707584; (b) Yan, M.; Kawamata, Y.; Baran, P. S. *Chem. Rev.* **2017,** *117*, 13230-13319.
(26) Molina, Á.; Laborda, E.; Gómez-Gil, J. M.; Martínez-Ortiz, F.; Compton, R. G. *Electrochim. Acta* **2016,** *195*, 230-245.
(27) Frisch, J.; Trucks, G. W.; Schegel, H. B.; Scuseria, G. E.; Robb, M. A.; Cheeseman, J. R.; Scalmani, G.; Barone, V.; Mennucci, B.; Petersson, G. A.; Nakatsuji, H.; Caricato, M.; Li, X.; Hratchian, H. P.;

Izmaylov, A.; Bloino, J.; Zheng, G.; Sonnenberg, J. L.; Hada, M.; Ehara, M.; Toyota, K.; Fukuda, R.; Hasegawa, J.; Ishida, M.; Nakajima, N.; Honda, Y.; Kitao, O.; Nakai, H.; Vreven, T.; Montgomery, J. A.; Jr. Peralta, J. E.; Ogliaro, F.; Bearpark, M.; Heyd, J. J.; Brothers, E.; Kudin, K. N.; Staroverov, V. N.; Keith, T.; Kobayashi, R.; Normand, J.; Raghavachari, K.; Rendell, A.; Burant, J. C.; Iyengar, S. S.; Tomasi, J.; Cossi, M.; Rega, N.; Millam, J. M.; Klene, M.; Knox, J. E.; Cross, J. B.; Bakken, V.; Adamo, C.; Jaramillo, J.; Gomperts, R.; Stratmann, R. E.; Yazyev, O.; Austin, A. J.; Cammi, R.; Pomelli, C.; Ochterski, J. W.; Martin, R. L.; Morokuma, K.; Zakrzewski, V. G.; Voth, G. A.; Salvador, P.; Dannenberg, J. J.; Dapprich, S.; Daniels, A. D.; Farkas, O.; Foresman, J. B.; Ortiz, J. V.; Cioslowski, J.; Fox, J. *Rev. D. Gaussian 09, Gaussian, Inc., Wallingford CT.* **2013**.

(28) Alecu, I.; Zheng, J.; Zhao, Y.; Truhlar, D. G. *J. Chem. Theory Comput.* **2010,** *6*, 2872-2887.

(29) Curtiss, L. A.; Raghavachari, K.; Redfern, P. C.; Baboul, A. G.; Pople, J. A. *Chem. Phys. Lett.* **1999,** *314*, 101-107.

(30) (a) Izgorodina, E. I.; Coote, M. L. *J. Phys. Chem. A* **2006,** *110*, 2486-2492; (b) Izgorodina, E. I.; Brittain, D. R.; Hodgson, J. L.; Krenske, E. H.; Lin, C. Y.; Namazian, M.; Coote, M. L. *J. Phys. Chem. A* **2007,** *111*, 10754-10768.

(31) Marenich, A. V.; Cramer, C. J.; Truhlar, D. G. *J. Phys. Chem. B* **2009,** *113*, 6378-6396.

(32) (a) Klamt, A. *J. Phys, Chem.* **1995,** *99*, 2224-2235; (b) Klamt, A.; Jonas, V.; Bürger, T.; Lohrenz, J. C. *J. Phys. Chem. A* **1998,** *102*, 5074-5085; (c) Klamt, A., *COSMO-RS: from quantum chemistry to fluid phase thermodynamics and drug design*. Elsevier: 2005.

(33) Louwen, J. N.; Pye, C. C.; Van Lenthe, E.; McGarrity, E. S.; Xiong, R.; Sandler, S. I.; Burnett, R. I., In http://www.scm.com, ADF2014 COSMO-RS, SCM, Theoreoretical Chemistry, Vrije Universiteit, Amsterdam, The Netherlands: 2014.

(34) Pye, C. C.; Ziegler, T.; Van Lenthe, E.; Louwen, J. N. *Can. J. Chem.* **2009,** *87*, 790-797.

(35) (a) Werner, H. J.; Knowles, P. J.; Knizia, G.; Manby, F. R.; Schütz, M. *WIREs Comput. Mol. Sci.* **2012,** *2*, 242-253; (b) Werner, H. J.; Knowles, P. J.; Knizia, G.; Manby, F. R.; Schütz, M.; Celani, P.; Györffy, W.; Kats, D.; Korona, T.; Lindh, R.; Mitrushenkov, A.; Rauhut, G.; Shamasundar, K. R.; Adler, T. B.; Amos, R. D.; Bernhardsson, A.; Berning, A.; Cooper, D. L.; Deegan, M. J. O.; Dobbyn, A. J.; Eckert, F.; Goll, E.; Hampel, C.; Hesselmann, A.; Hetzer, G.; Hrenar, T.; Jansen, G.; Köppl, C.; Liu, Y.; Lloyd, A. W.; Mata, R. A.; May, A. J.; McNicholas, S. J.; Meyer, W.; Mura, M. E.; Nicklass, A.; O'Neill, D. P.; Palmieri, P.; Peng, D.; Pflüger, K.; Pitzer, R.; Reiher, M.; Shiozaki, T.; Stoll, H.; Stone, A. J.; Tarroni, R.; Thorsteinsson, T.; Wang, M. *MOLPRO, version 2015.1, a package of ab initio programs,* http://www.molpro.net **2015**.